

Diels–Alder Reactions of Graphene: Computational Predictions of Products and Sites of Reaction

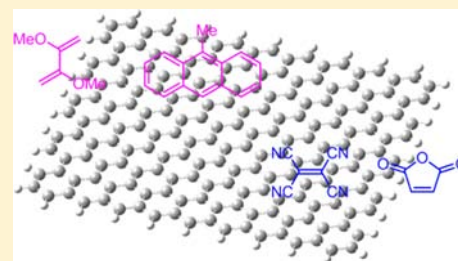
Yang Cao,[†] Sílvia Osuna,[†] Yong Liang,[†] Robert C. Haddon,[‡] and K. N. Houk^{*,†}

[†]Department of Chemistry and Biochemistry, University of California, Los Angeles, California 90095, United States

[‡]Department of Chemistry and Chemical & Environmental Engineering, University of California, Riverside, California 92521, United States

S Supporting Information

ABSTRACT: The cycloaddition reactions and noncovalent π interactions of 2,3-dimethoxybutadiene (DMBD), 9-methylanthracene (MeA), tetracyanoethylene (TCNE), and maleic anhydride (MA) with graphene models have been investigated using density functional theory (DFT) calculations. Reaction enthalpies have been obtained to assess the reactivity and selectivity of covalent and noncovalent functionalization. Results indicate that graphene edges may be functionalized by the four reagents through cycloaddition reactions, while the interior regions cannot react. Noncovalent complexation is much more favorable than cycloaddition reactions on interior bonds of graphene. The relative reactivities of different sites in graphene are related to loss of aromaticity and can be predicted using Hückel molecular orbital (HMO) localization energy calculations.



INTRODUCTION

Chemical functionalization is a method to manipulate the electronic properties of graphene.¹ By forming covalent bonds and converting sp^2 - into sp^3 -hybridized carbons, the electronic properties of graphene can be tuned, and additional functionality can be incorporated. However, graphene is a highly stabilized, intrinsically inert, macromolecular aromatic material. To overcome the large reaction barrier, highly reactive chemical reagents or harsh reaction conditions are often required,^{1,2} as in examples such as oxidation,^{3–5} fluorination,^{6–8} hydrogenation,^{9–11} and radical addition.^{12,13} Inspired by well-established modifications of fullerenes and carbon nanotubes, cycloaddition reactions are another approach to the chemical functionalization of graphene. Nitrenes, which are reactive intermediates that can be obtained from the decomposition of azides, are reported to undergo (2 + 1) cycloaddition reactions on graphene and form aziridines.^{14,15} Benzyne have been reported to modify graphene surfaces efficiently with a high degree of functionalization through (2 + 2) cycloaddition pathways.^{16,17} The 1,3-dipolar cycloaddition of an azomethine ylide has also been reported to functionalize graphene.^{18,19}

In 2011, Haddon's group reported a series of Diels–Alder (DA) reactions on graphene.^{20,21} It was reported that graphene reacts reversibly as a dienophile with 2,3-dimethoxybutadiene (DMBD) or 9-methylanthracene (MeA). The DA reaction of DMBD with graphene could be achieved both in solution at 120 °C and in the gas phase at 50 °C. Both reactions are reported to reverse at 170 °C. MeA reacts with graphene in a solution of *p*-xylene at 130 °C, and the retro-DA reaction occurs at 160 °C. Graphene is also reported to react as a diene with tetracyanoethylene (TCNE) and with maleic anhydride (MA). The reaction with TCNE proceeds at room temperature

and reverses at 100 °C. MA requires 120 °C for the DA reaction and reverses at 150 °C. Raman spectroscopy was mainly employed to track the reaction process. The ratio of D to G band intensity (I_D/I_G) was considered as an index of the degree of functionalization.

The noncovalent functionalization of graphene by π complexes has also been studied extensively.¹ The graphene surface is known to adsorb many types of molecules through noncovalent interactions, from metal ions to small organic molecules to biomolecules such as DNA and proteins.^{22–25} The electronic properties of graphene can be effectively modified by adding adsorbate molecules to the surface and forming charge transfer complexes.^{26,27} Rao and co-workers found that TCNE and graphene formed a charge transfer complex in the solution phase, where TCNE was an electron acceptor and graphene functioned as an electron donor.^{28–31} Raman spectroscopy was again utilized as a major characterization tool.²⁸ Through comparing the Raman spectra before and after the interaction with TCNE, they found that the intensity of the D band increased after the complex formation, as did the I_D/I_G ratio. The increased I_D/I_G ratio phenomenon was also observed in the interaction of graphene with electron donor molecules. Both covalent and noncovalent bonding could increase the D band intensity in the Raman spectrum.

To better understand the reactivity and selectivity of the four reagents (DMBD, MeA, TCNE, and MA) with graphene, we have performed a computational assessment through DFT calculations. Our graphene models are finite-size polybenzenoid (25 fused benzene rings) hydrocarbons with no considerations

Received: October 4, 2013

Published: October 25, 2013

of complex defects. Reactivities in the interior and peripheral sites (zigzag and armchair edges) are considered. We evaluated the feasibility of (2 + 2), (4 + 2), and (4 + 4) cycloadditions, where graphene functions as a 2π or 4π component. We also studied the noncovalent interactions of the four compounds with graphene. We assessed the radical character of graphene fragments by spin density calculations. HMO theory provides insights into relative reactivities of different sites in graphene.

Before the submission of this paper, Denis reported a study of Diels–Alder reactions of graphene with the same dienes or dienophiles studied here.³² Although different models and density functional methods were used, the conclusions about the unreactivity of the interior portion of graphene in Diels–Alder reactions are congruent with our results.

■ COMPUTATIONAL MODELS AND METHODS

Ideal graphene has a locally perfectly flat, single-layer structure comprised of purely sp^2 -hybridized carbons.³³ Graphene flakes generally have several thousand carbons. In a large graphene flake, the carbons are indistinguishable and are packed into a honeycomb lattice with a C–C bond length of 1.42 Å.³⁴ However, real graphene samples inevitably have defects and vary in size, layers, and boundary conditions, depending on their fabrication processes. Enormous efforts at fabrication have been made in recent years to prepare pristine graphene, but still there are significant variations in graphene structures and qualities. Graphene samples with lateral dimensions ranging from 2 nm (a few hundred carbon atoms)³⁵ up to 1 mm³⁶ have been reported. There are two basic shapes for graphene edges: zigzag and armchair.³⁶ A previous study indicated that zigzag edges have multiradical character and are predicted to have high reactivity.³⁷ Scott's group also reported the Diels–Alder reaction of acetylene to the armchair edge of aromatic hydrocarbons.³⁸ We have studied two graphene models containing both types of edges. They are polybenzenoid hydrocarbons $C_{70}H_{22}$ (25 fused benzene rings). Figure 1 shows structures of the two graphene models: model 1 terminates

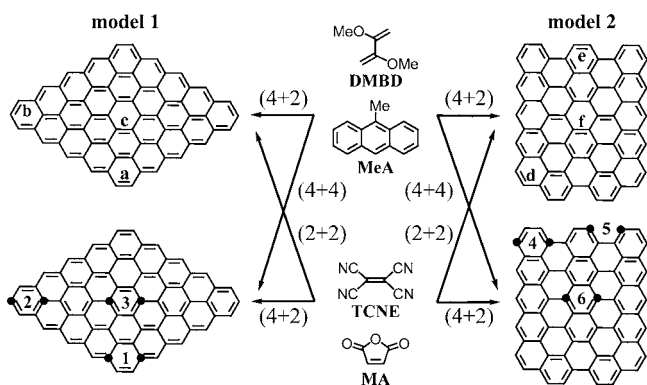


Figure 1. Two graphene models (models 1 and 2) terminated with hydrogen atoms. Reaction sites including interior and peripheral bonds are considered. When graphene functions as the 2π component, six bonds from a to f are considered. When graphene functions as the 4π component, six reaction sites from 1 to 6 are calculated.

with a zigzag edge and model 2 has armchair edges. They are both terminated with hydrogen atoms. Denis found that unsaturated edges are much more reactive than edges saturated with hydrogen atoms.³² He also found that the presence of Stone–Wales translocations, 585 double vacancies, and 555–777 reconstructed double vacancies did not significantly change graphene reactivity.³²

For computational investigations, the larger the model is, the more closely it resembles graphene. However, DFT computation times scale by about n^4 (n = number of atoms) as the size increases, which greatly limits the size of models.^{39–41} In a previous study, we performed benchmarks regarding the size effects on graphene models.⁴² It was

found that, for both interior and peripheral bonds, the energetics quickly converged as the model size increases. This indicates that our finite-size models provide reliable energetics for both interior and peripheral bonds.

Reactions of interior and peripheral bonds in graphene are considered. When graphene functions as the 2π component, three representative bonds from each model are studied. The bonds a and b represent zigzag edges. Ideally, the two zigzag bonds are indistinguishable when the graphene model approaches infinite. Here, in our finite-size model, they differ in reactivity. Bonds a and b are most reactive in these two categories, respectively. The corner bond a in model 1 can also be viewed as the joint part of zigzag and armchair edges of graphene. The interior bond c comprises the majority of bonds in graphene. Likewise, the peripheral bond d in model 2 can be viewed as the joint part of zigzag and armchair edges of graphene. Due to the similarities of their structure environments, the d bond is expected to have reactivity comparable with that of a. The edge bond e in model 2 represents the armchair edge. The interior bond f represents the graphene interior. In addition to the DA reactions ((4 + 2) reactions with DMBD and MeA), we also considered the possibilities of (2 + 2) cycloaddition reactions toward TCNE and MA. Likewise, when graphene functions as the 4π component, DFT calculations were conducted on another six sites. In particular, site 5 is a representative armchair edge that is similar to the bay region of Scott's models.³⁸ Interior sites 3 and 6 represent the graphene interior. The (4 + 2) cycloaddition reactions with TCNE and MA, as well as the (4 + 4) reactions with DMBD and MeA, were conducted on these sites.

A previous computational study from our group indicates that polyacenes possess an open-shell singlet ground state.⁴³ The polyradical behavior was also found in graphene nanoflakes with system sizes on the order of 100 carbon atoms.³⁷ Our calculation is in agreement with previous findings that graphene models are more stable as open-shell singlet states than as closed-shell singlet and open-shell triplet states.⁴⁴ The open-shell character requires unrestricted DFT calculations for species involving graphene. All calculations were performed with Gaussian 09.⁴⁵ The geometry optimizations of all the minima were carried out at the (U)M06-2X level of theory^{46,47} with the 6-31G(d) basis set.⁴⁸ Single-point energy calculations were subsequently carried on the optimized structures at the (U)M06-2X and (U) ω B97X-D levels⁴⁹ with the larger basis set 6-311G(d,p). Both methods yield better results when describing medium- to long-range electron correlation and dispersion effects than traditional hybrid DFT methods such as B3LYP.^{46,49} M06-2X is reported to provide reliable energetics for cycloaddition reactions.⁵⁰ Very recently, M06-2X has also been demonstrated to generate good results for calculating the adsorption enthalpies of small organic molecules on graphene.⁵¹ Vibrational frequencies were computed at the (U)M06-2X/6-31G(d) level to check whether each optimized structure is an energy minimum and to evaluate zero-point vibrational energies (ZPVE) and thermal corrections at 298 K. Here only (U)M06-2X results will be discussed. The (U) ω B97X-D results are provided in the Supporting Information, which gave similar energetics and the same general conclusions.

It is well-known that, for bimolecular reactions, the free energy term (ΔG) is unfavorable due to the entropy contribution ($\Delta G = \Delta H - T\Delta S$; $-T\Delta S$ is positive). Recently, it was reported that the entropy contribution is small (within 5 kcal/mol) from calculations on free energies of the noncovalent association of graphene with small organic molecules.²⁵ This corresponds to a ΔS of about -15 eu (cal/(mol K)), appropriate for loss of one translational and two rotational degrees of freedom. Consequently, a complex of a small molecule at graphene will be exergonic if ΔH is about -5 kcal/mol or more exothermic. For a covalent cycloadduct, the ΔS will be -30 eu or even more negative so that a ΔH of reaction of -10 kcal/mol or more exothermic will be necessary for an exergonic reaction. We use enthalpies to evaluate the feasibility of reactions, as the entropy term in ΔG is overestimated by gas-phase calculations based on harmonic frequencies.

RESULTS AND DISCUSSION

2,3-Dimethoxybutadiene (DMBD). Figure 2 shows the product structures and reaction enthalpies for Diels–Alder

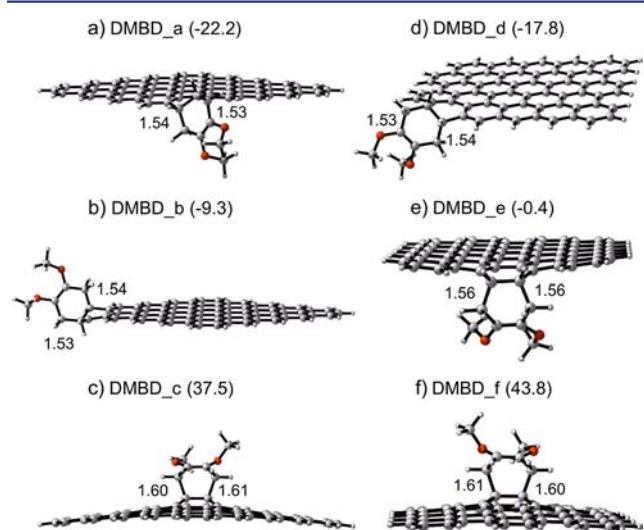


Figure 2. Diels–Alder adducts of DMBD with graphene on bonds a–c in model 1 and d–f in model 2, where graphene functions as a dienophile. Reaction enthalpies are given in kcal/mol. The C–C bond lengths are given in Å.

reactions between DMBD and two graphene models, where graphene functions as a dienophile. The peripheral bonds a and d are relatively reactive with comparable reaction enthalpies of -22.2 and -17.8 kcal/mol, respectively. The zigzag edge b and armchair edge e are slightly reactive with enthalpies of -9.3 and -0.4 kcal/mol. However, interior bonds c and f are inert with highly endothermic reaction enthalpies of 37.5 and 43.8 kcal/mol. The DA reactions at interior bonds are highly endothermic, due to the aromaticity breaking and curvature introduction. The reaction on the interior bond has a direct impact on four local benzene rings. Through comparison of the product morphology shown in Figure 2, it is clearly seen that obvious curvature is introduced at the tetrahedral atoms where two new C–C bonds formed. This suggests that DMBD can functionalize graphene edges or defects through DA reactions, while the interior areas will not react at all. When DMBD reacts with graphene through the (4 + 4) cycloaddition on sites 1–3 in model 1 and 4–6 in model 2, these six reactions are all unfavorable with reaction enthalpies ranging from 12.8 to 57.1 kcal/mol. The product structures and reaction enthalpies are provided in Figure S1 (see the Supporting Information). Overall, the (4 + 4) cycloaddition of DMBD with graphene is not feasible at edges or interior sites.

In addition to cycloaddition reactions, we also assessed the feasibility of the formation of DMBD–graphene complexes. Figure 3 shows the structures of DMBD–graphene complexes in two graphene models from two viewpoints (top and side). DMBD retains the *s-trans* conformation, and the distance between DMBD and graphene is about 3.2 Å. The binding enthalpies from the two models are very close: -14.9 and -15.7 kcal/mol, respectively. Recently, Otyepka and co-workers performed a combined experimental and theoretical exploration of the adsorption of seven small organic molecules onto graphene.⁵¹ The experimental adsorption enthalpies of seven organic molecules on graphene were obtained from gas

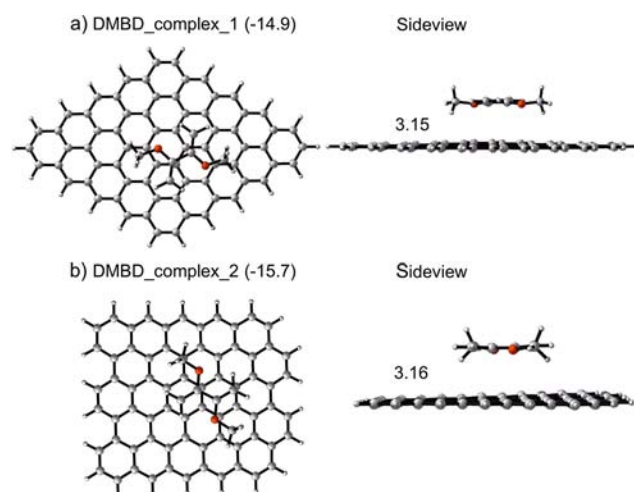


Figure 3. DMBD–graphene complex structures in both models from two viewpoints. The binding enthalpies are given in kcal/mol. The distances are given in Å.

chromatography measurements and spanned from -5.9 (dichloromethane) to -13.5 kcal/mol (toluene). Quantum mechanical calculations were conducted on a coronene model to calculate theoretical interaction energies. M06-2X gives a mean error of 0.8 kcal/mol from the gold-standard CCSD(T) method.⁵¹ Therefore, our M06-2X calculations are believed to give reliable energetics for the formation of complexes on graphene. In addition, it is found that noncovalent graphene complexes are predominantly stabilized by dispersion, which contributes more than 60% to the attractive energy, even in polar complexes.⁵¹ Our calculations show that, for DMBD, noncovalent binding (Figure 3) is less exothermic than the DA functionalization on the edge bonds a/d (Figure 2). The covalent functionalization on the graphene edges is preferred over the π complex. In contrast, the DA reaction at the interior, which consists of the majority of graphene bonds, is highly endothermic (around 40 kcal/mol; Figure 2). Formation of the DMBD–graphene complex is exothermic by about 15 kcal/mol (Figure 3); therefore, the π complex is preferred over cycloaddition reactions on the interior of the graphene surface.

9-Methylanthracene (MeA). The same calculations were performed on the MeA molecule. Figure 4 shows the product structures and reaction enthalpies for Diels–Alder reactions between MeA and graphene models, where graphene functions as a dienophile. In general, reactions of MeA are less exothermic than these of DMBD, because MeA forms strained bicyclo[2.2.2]octadiene adducts. The edge bonds a, b, and d may react, as their reaction enthalpies are below 0 kcal/mol (Figure 4). The armchair edge e is barely reactive with an enthalpy of 4.9 kcal/mol. Highly endothermic enthalpies (over 39 kcal/mol) in interior bonds c and f are obtained, indicating that MeA could not functionalize the graphene surface through DA reactions. We also calculated the (4 + 4) reactions between MeA and graphene models. All of the reaction enthalpies are highly endothermic, even on the edges. This suggests that the (4 + 4) cycloadditions are highly unfavorable. The product structures and reaction enthalpies are provided in Figure S2 (see the Supporting Information).

The MeA–graphene noncovalent complex is much easier to form. Figure 5 shows the structure of MeA–graphene complexes in two graphene models from two viewpoints (top and side). The binding enthalpies from both models are quite

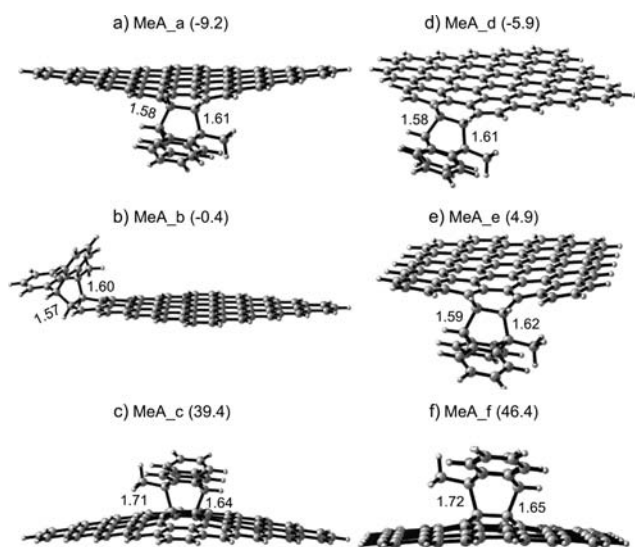


Figure 4. Diels–Alder adducts of MeA with graphene on bonds a–c in model 1 and d–f in model 2, where graphene functions as a dienophile. Reaction enthalpies are given in kcal/mol. The C–C bond lengths are given in Å.

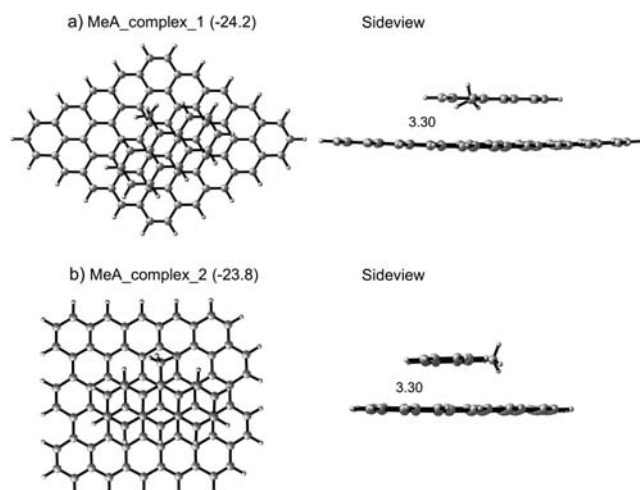


Figure 5. MeA–graphene complex structures in both models from two viewpoints. The binding enthalpies are given in kcal/mol. The distances are given in Å.

large, around -24 kcal/mol, and are more favorable than the most reactive DA functionalization on bond a (-9.2 kcal/mol, Figure 4). MeA itself is an aromatic molecule, forming π – π stacking between graphene with a distance of 3.30 Å. The noncovalent interaction of graphene and anthracene was studied before. Lee and co-workers utilized the noncovalent interaction between 9-anthracenecarboxylic acid and graphene to prepare stable aqueous graphene at room temperature.⁵² The anthracene-modified graphene material was found to have good electrochemical properties for supercapacitor applications.⁵³ Such a stable π – π stacking interaction was also reported in other aromatic molecules on graphene.^{26,54} Graphene functionalized by aromatic molecules is easily dispersible for solution processing. More importantly, the π – π stacking interaction is a promising method to control the electronic properties of graphene, such as opening the band gap, optimizing the charge carrier type, and so on.²⁶ Here our calculations indicate that, for the MeA molecule, the noncovalent interaction with graphene

is significant, in agreement with the above experiments. Although the DA functionalization might occur on certain edges or defects, the noncovalent complex is preferred.

Tetracyanoethylene (TCNE). For graphene reactions with the electron-deficient 2π components TCNE and maleic anhydride (MA), both $(4 + 2)$ and $(2 + 2)$ pathways were considered. Figure 6 shows the product structures and reaction

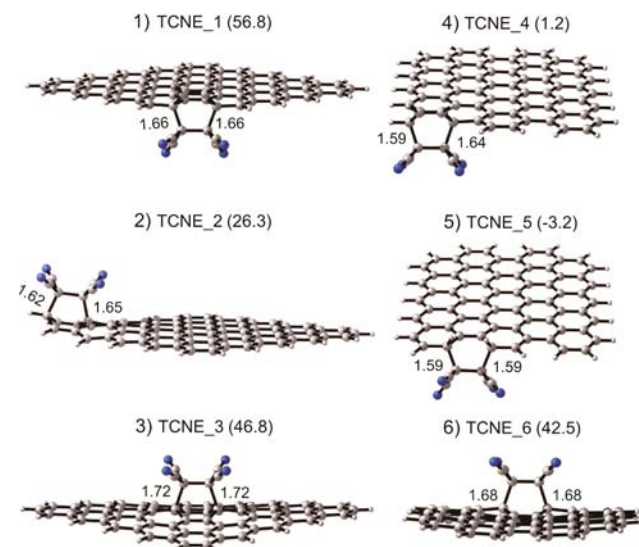


Figure 6. Diels–Alder adducts of TCNE with graphene on sites 1–3 in model 1 and 4–6 in model 2, where graphene functions as a diene. Reaction enthalpies are given in kcal/mol. The C–C bond lengths are given in Å.

enthalpies for Diels–Alder reactions between TCNE and two graphene models. The DA reactions of dienes 1–3 in model 1 are all energetically unfavorable, with reaction enthalpies from 26.3 to 56.8 kcal/mol. The zigzag edges of graphene cannot function as a diene in this reaction. The armchair edge 5 resembles the bay region reported by Scott.³⁸ The reaction of TCNE at this site has a slightly negative reaction enthalpy, -3.2 kcal/mol. The interior site 6 is unfeasible with an enthalpy of 42.5 kcal/mol.

TCNE is also known to react with electron-rich alkenes to give $(2 + 2)$ adducts.⁵⁵ We tested the energetics of $(2 + 2)$ adducts, as shown in Figure 7. Six graphene bonds, a–f, were considered as 2π components in $(2 + 2)$ reactions with TCNE. Only peripheral bonds a and d react favorably, with enthalpies of -10.4 and -6.8 kcal/mol, respectively. The reactions on interior bonds c and f are endothermic by 38.9 and 45.1 kcal/mol. Therefore, TCNE could selectively functionalize graphene edges and defects through $(2 + 2)$ or $(4 + 2)$ reactions. However, interior areas will not react, due to the highly unfavorable reaction energetics.

Figure 8 shows TCNE–graphene complexes that are formed with a quite short distance of about 3.1 Å. In addition, Mulliken charge analysis shows that there is partial charge ($0.05e$) transfer from graphene to TCNE within their noncovalent complexes. The complexes from the two models have binding enthalpies of -16.1 and -16.4 kcal/mol, respectively. Rao's group has systematically studied the interaction of electron-donor and -acceptor molecules with graphene and single-walled carbon nanotubes. An experimental binding free energy has been measured to be -5.7 kcal/mol for TCNE and graphene in solution from isothermal titration calorimetry (ITC) measure-

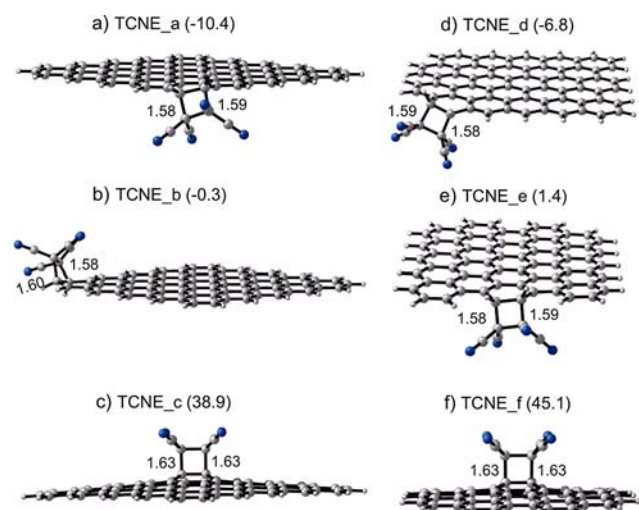


Figure 7. (2 + 2) adducts of TCNE with graphene on bonds a–c in model 1 and d–f in model 2, where graphene functions as a 2π component. Reaction enthalpies are given in kcal/mol. The C–C bond lengths are given in Å.

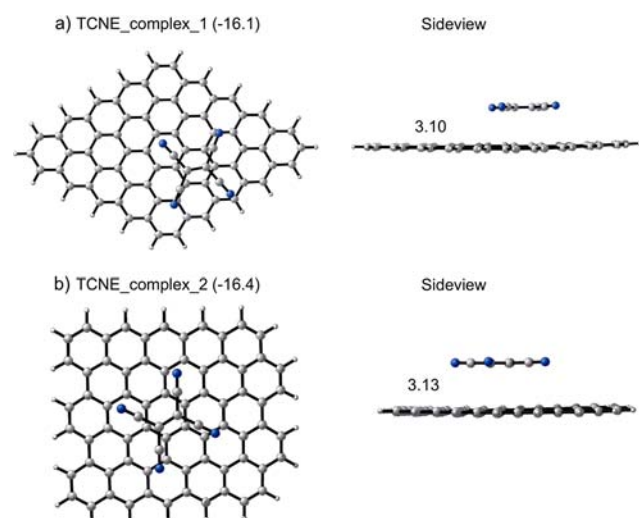


Figure 8. TCNE–graphene complex structures in both models from two viewpoints. The binding enthalpies are given in kcal/mol. The distances are given in Å.

ments.²⁹ This is in agreement with our DFT calculations, considering that the entropy contribution in solution is 5–10 kcal/mol. They found that the single-walled carbon nanotubes interacted reversibly with TCNE through charge transfer interactions. The noncovalent functionalization by TCNE has a significant impact on the electronic properties of metallic carbon nanotubes, with an opening in band gap and changes in Raman spectral features.²⁹ A similar impact is expected on graphene. Both electron donors (tetrathiafulvalene) and electron acceptors (TCNE) establish charge transfer interactions with graphene, and the changes in Raman spectral features of graphene were reported upon the noncovalent functionalization of TCNE.²⁸ These experimental observations support our computational results that the van der Waals complex is the dominant product of the reaction of TCNE with graphene.

Maleic Anhydride (MA). The reactions of MA were also explored. For DA reactions, only armchair edges 4 and 5 in

model 2 show exothermic enthalpies of –2.8 and –9.8 kcal/mol. The reaction enthalpies on the two zigzag edges 1 and 2 are both more than 22 kcal/mol. The reactions on interior bonds in both models are about 40 kcal/mol (Figure S3; see the Supporting Information). For the (2 + 2) cycloadditions, edge bonds a and d show slightly favorable enthalpies of –7.1 and –4.2 kcal/mol, respectively. Reactions of interior bonds c and f are endothermic by around 40 kcal/mol (Figure S4, Supporting Information). Therefore, the interior bonds of graphene cannot be functionalized by MA through cycloadditions. Very recently, Baek and co-workers reported Diels–Alder reactions on graphite through dry ball-milling in the presence of MA, in which graphite functions as the diene and MA as the dienophile.⁵⁶ They found that the DA adducts are edge-selective. This is in agreement with our calculation results. The complex between MA and graphene is formed with a distance of 3.10 Å and is exothermic by about –11 kcal/mol (Figure 9). This suggests that noncovalent complex formation is also dominant with MA.

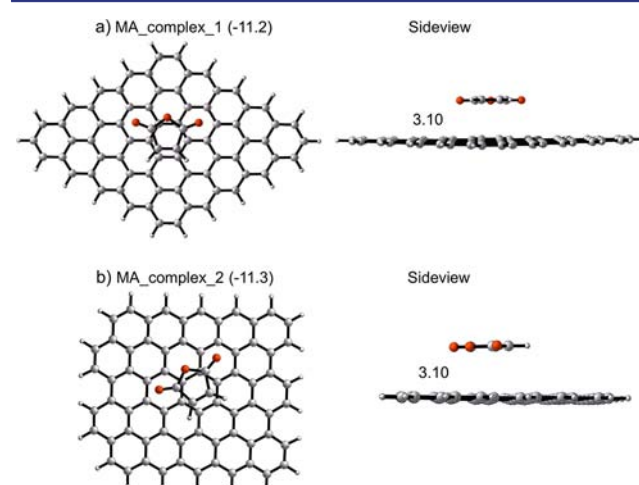


Figure 9. MA–graphene complex structures in both models from two viewpoints. The binding enthalpies are given in kcal/mol. The distances are given in Å.

Computed Indicators of Reactivity. Jiang and co-workers reported that, for graphene nanoribbons, the unpaired π electrons are distributed mainly on zigzag edges.⁵⁷ The partial radical character is related to the high chemical reactivity of zigzag edges in comparison to interior bonds and armchair edges of graphene.⁵⁸ Similar phenomena were reported by Lischka and co-workers.³⁷ We have calculated the spin densities of two graphene models, as shown in Figure 10, using

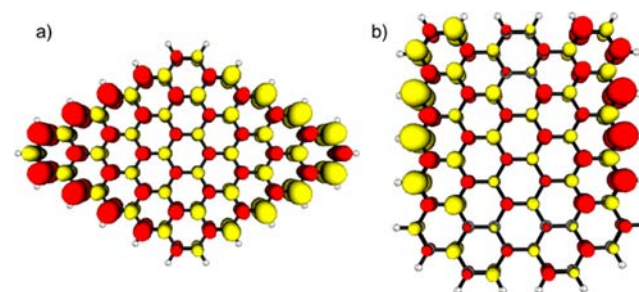


Figure 10. UM06-2X-computed spin densities for graphene models 1 (a) and 2 (b).

unrestricted M06-2X calculations. The unpaired electron density is mainly distributed on the edges in both models. Model 2 has two zigzag edges and two armchair edges. The unpaired π electron density is highest on the zigzag edges. This is in agreement with previous studies and qualitatively explains why edges are generally much more reactive than interior regions.

We have also evaluated the reactivities of graphene using localization energies calculated by simple Hückel molecular orbital (HMO) theory. While very approximate, HMO does give a good account for reactivities of different aromatic hydrocarbons. The energy of π electrons is expressed in terms of α and β : $E = n\alpha + \lambda\beta$. α is the Coulomb integral, and β is the resonance integral. The localization energy (E_L) was recognized and developed by Wheland⁵⁹ and Brown⁶⁰ in the 1940–1950s. By definition, it is the energy difference between the residual molecule (E_r) and the original π system (E): $E_L = E_r - E$. Here, in our systems, the residual molecule is that remaining after the two reacting carbon atoms of the graphene are removed from models 1 and 2 (Figure 1). The localization energy qualitatively correlates with the reactivity of aromatic substitution reactions.⁶⁰ The most reactive position has the smallest localization energy. We calculated the HMO energies using SHMO.⁶¹ Table 1 summarizes the localization energies for our two graphene models. The 2α term is neglected, as it is the same for all reactions.

Table 1. HMO Localization Energies for Graphene Models Shown in Figure 1 (in Units of $-\beta$)

| bond | E_L | site | E_L |
|------|-------|------|-------|
| a | 3.0 | 1 | 5.5 |
| b | 3.3 | 2 | 4.6 |
| c | 4.4 | 3 | 5.1 |
| d | 3.1 | 4 | 4.2 |
| e | 3.3 | 5 | 3.9 |
| f | 4.6 | 6 | 4.9 |

When graphene functions as a 2π component, bonds a–c in model 1 and bonds d–f in model 2 are considered. Bond a is the most reactive with the smallest localization value of 3.0. Bond d, with close reactivity to a, has a value of 3.1. The interior bonds c and f are the most inert, as indicated by their localization values of 4.4 and 4.6, respectively. In the case of graphene acting as a 4π component, sites 1–3 in model 1 and sites 4–6 in model 2 are considered. Although site 1 is in the edge, it is the least reactive with the largest value of 5.5. Site 5 with a value of 3.9 is the most reactive. In both models, interior regions of graphene are substantially more inert than active edges. These are all in agreement with the DFT calculations reported. This suggests that the reactivities of different graphene sites are largely determined by the loss of aromaticity energies after functionalization. The HMO theory can quickly provide information for the prediction of the reaction sites on graphene fragments of any size.

CONCLUSION

We have calculated the cycloaddition reactions and non-covalent interactions of four reagents (DMBD, MeA, TCNE, and MA) on two graphene models. The interior bonds in both models, which resemble most of the bonds in graphene, cannot be directly functionalized through cycloaddition reactions by these four reagents, due to their highly unfavorable reaction

enthalpies. DMBD and MeA could react with graphene edges through (4 + 2) cycloadditions. Both (4 + 2) and (2 + 2) reaction pathways may be feasible between TCNE/MA and graphene edges. The enthalpies of noncovalent interactions of these four molecules range from -11.2 to -24.2 kcal/mol. Except for the DMBD molecule, the binding interactions of the other three molecules are all more favorable than their cycloaddition counterparts, even on reactive edge bonds. This suggests that the noncovalent interaction is dominant on graphene interior regions. We also performed spin density and HMO calculations on our graphene models. The spin density diagram shows multiradical character on the edges, especially the zigzag edges. We found that Hückel molecular orbital (HMO) localization energies can be used to predict the relative reactivities of different sites in graphene.

ASSOCIATED CONTENT

Supporting Information

Figures S1–S4 and tables giving computational details. This material is available free of charge via the Internet at <http://pubs.acs.org>.

AUTHOR INFORMATION

Corresponding Author

E-mail for K.N.H.: houk@chem.ucla.edu.

Notes

The authors declare no competing financial interest.

ACKNOWLEDGMENTS

We are grateful to the National Science Foundation (CHE-1059084) for financial support of this research. S.O. acknowledges the European Community for a postdoctoral fellowship (PIOF-GA-2009-252856). Calculations were performed on the Hoffman2 cluster at UCLA and the Extreme Science and Engineering Discovery Environment (XSEDE), which is supported by the NSF (OCI-1053575).

REFERENCES

- Georgakilas, V.; Otyepka, M.; Bourlinos, A. B.; Chandra, V.; Kim, N.; Kemp, C. K.; Hobza, P.; Zboril, R.; Kim, K. S. *Chem. Rev.* **2012**, *112*, 6156–6214.
- Loh, K. P.; Bao, Q.; Ang, P. K.; Yang, J. *J. Mater. Chem.* **2010**, *20*, 2277–2289.
- Hummers, W. S.; Offenman, R. E. *J. Am. Chem. Soc.* **1958**, *80*, 1339–1339.
- Chattopadhyay, J.; Mukherjee, A.; Hamilton, C. E.; Kang, J. H.; Chakraborty, S.; Guo, W.; Kelly, K. F.; Barron, A. R.; Billups, W. E. *J. Am. Chem. Soc.* **2008**, *130*, 5414–5415.
- Cote, L. J.; Cruz-Silva, R.; Haug, J. *J. Am. Chem. Soc.* **2009**, *131*, 11027–11032.
- Worsley, K. A.; Ramesh, P.; Mandal, S. K.; Niyogi, S.; Itkis, M. E.; Haddon, R. C. *Chem. Phys. Lett.* **2007**, *445*, 51–56.
- Robinson, J. T.; Burgess, J. S.; Junkermeier, C. E.; Badescu, S. C.; Reinecke, T. L.; Perkins, F. K.; Zalalutdniov, M. K.; Baldwin, J. W.; Culbertson, J. C.; Sheehan, P. E.; Snow, E. S. *Nano Lett.* **2010**, *10*, 3001–3005.
- Bon, S. B.; Valentini, L.; Verdejo, R.; Fierro, J. L. G.; Peponi, L.; Lopez-Manchado, M. A.; Kenny, J. M. *Chem. Mater.* **2009**, *21*, 3433–3438.
- Ryu, S.; Han, M. Y.; Maultzsch, J.; Heinz, T. F.; Kim, P.; Steigerwald, M. L.; Brus, L. E. *Nano Lett.* **2008**, *8*, 4597–4602.
- Balog, R.; Jørgensen, B.; Nilsson, L.; Andersen, M.; Rienks, E.; Bianchi, M.; Fanetti, M.; Lægsgaard, E.; Baraldi, A.; Lizzit, S.; Slijivancanin, Z.; Besenbacher, F.; Hammer, B.; Pedersen, T. G.; Hofmann, P.; Hornekær, L. *Nat. Mater.* **2010**, *9*, 315–319.

- (11) Yang, Z.; Sun, Y.; Alemany, L. B.; Narayanan, T. N.; Billups, W. *J. Am. Chem. Soc.* **2012**, *134*, 18689–18694.
- (12) Lomeda, J. R.; Doyle, C. D.; Kosynkin, D. V.; Hwang, W. F.; Tour, J. M. *J. Am. Chem. Soc.* **2008**, *130*, 16201–16206.
- (13) Bekyarova, E.; Itkis, M. E.; Ramesh, P.; Berger, C.; Sprinkle, M.; de Heer, W. A.; Haddon, R. C. *J. Am. Chem. Soc.* **2009**, *131*, 1336–1337.
- (14) Liu, L.-H.; Yan, M. *Nano Lett.* **2009**, *9*, 3375–3378.
- (15) Strom, T. A.; Dillon, E. P.; Hamilton, C. E.; Barron, A. R. *Chem. Commun.* **2010**, *46*, 4097–4099.
- (16) Zhong, X.; Jin, J.; Li, S.; Niu, Z.; Hu, W.; Li, R.; Ma, J. *Chem. Commun.* **2010**, *46*, 7340–7342.
- (17) Denis, P. A.; Iribarne, F. *J. Mater. Chem.* **2012**, *22*, 5470–5477.
- (18) Quintana, M.; Spyrou, K.; Grzelczak, M.; Browne, W. R.; Rudolf, P.; Prato, M. *ACS Nano* **2010**, *4*, 3527–3533.
- (19) Georgakilas, V.; Bourlinos, A. B.; Zboril, R.; Steriotis, T. A.; Dallas, P.; Stubos, A. K.; Trapalis, C. *Chem. Commun.* **2010**, *46*, 1766–1768.
- (20) Sarkar, S.; Bekyarova, E.; Niyogi, S.; Haddon, R. C. *J. Am. Chem. Soc.* **2011**, *133*, 3324–3327.
- (21) Sarkar, S.; Bekyarov, E.; Haddon, R. C. *Acc. Chem. Res.* **2012**, *45*, 673–682.
- (22) Lu, C. H.; Yang, H. H.; Zhu, C. L.; Chen, X.; Chen, G. N. *Angew. Chem., Int. Ed.* **2009**, *48*, 4785–4787.
- (23) Shan, C. S.; Yang, H. F.; Song, J. F.; Han, D. X.; Ivaska, A.; Niu, L. *Anal. Chem.* **2009**, *81*, 2378–2382.
- (24) Baby, T. T.; Aravind, S. S. J.; Arockiadoss, T.; Rakhi, R. B.; Ramaprabhu, S. *Sens. Actuators B* **2010**, *145*, 71–77.
- (25) Haldar, S.; Kolar, M.; Sedlak, R.; Hobza, P. *J. Phys. Chem. C.* **2012**, *116*, 25328–25336.
- (26) Zhang, Z.; Huang, H.; Yang, X.; Zhang, L. *J. Phys. Chem. Lett.* **2011**, *2*, 2897–2905.
- (27) Ishikawa, R.; Bando, M.; Morimoto, Y.; Sandhu, A. *Nanoscale Res. Lett.* **2011**, *6*, 111.
- (28) Voggu, R.; Das, B.; Rout, C. S.; Rao, C. N. R. *J. Phys.: Condens. Matter* **2008**, *20*, 472204.
- (29) Varghese, N.; Ghosh, A.; Voggu, R.; Rao, C. N. R. *J. Phys. Chem. C.* **2009**, *113*, 16855–16859.
- (30) Choudhury, D.; Das, B.; Sarma, D. D.; Rao, C. N. R. *Chem. Phys. Lett.* **2010**, *497*, 66–69.
- (31) Rao, C. N. R.; Voggu, R. *Mater. Today* **2010**, *13*, 34–40.
- (32) Denis, P. A. *Chem. Eur. J.* **2013**, *19*, 15719–15725.
- (33) Geim, A. K.; Novoselov, K. S. *Nat. Mater.* **2007**, *6*, 183–191.
- (34) Heyrovská, R. *arXiv.org Physics* **2008**, arxiv.org/abs/0804.4086.
- (35) Ritter, K. A.; Lyding, J. W. *Nanotechnology* **2008**, *19*, 015704.
- (36) Jia, X.; Campos-Delgado, J.; Terrones, M.; Meunier, V.; Dresselhaus, M. S. *Nanoscale* **2011**, *3*, 86–95.
- (37) Plasser, F.; Pasalic, H.; Gerzabek, M. H.; Libisch, F.; Reiter, R.; Burgdorfer, J.; Müller, T.; Shepard, R.; Lischka, H. *Angew. Chem., Int. Ed.* **2013**, *52*, 2581–2584.
- (38) Fort, E. H.; Jeffreys, M. S.; Scott, L. T. *Chem. Commun.* **2012**, *48*, 8102–8104.
- (39) Strout, D. L.; Scuseria, G. E. *J. Chem. Phys.* **1995**, *102*, 8448–8452.
- (40) Pérez-Jordá, J. M.; Yang, W. *J. Chem. Phys.* **1997**, *107*, 1218–1226.
- (41) Krukau, A. V.; Scuseria, G. E.; Perdew, J. P.; Savin, A. *J. Chem. Phys.* **2008**, *129*, 124103.
- (42) Cao, Y.; Houk, K. N. *J. Mater. Chem.* **2011**, *21*, 1503–1508.
- (43) Bendikov, M.; Duong, H. M.; Starkey, K.; Houk, K. N.; Carter, E. A.; Wudl, F. *J. Am. Chem. Soc.* **2004**, *126*, 7416–7417.
- (44) Bian, S.; Scott, A. M.; Cao, Y.; Liang, Y.; Osuna, S.; Houk, K. N.; Braunschweig, A. B. *J. Am. Chem. Soc.* **2013**, *135*, 9240–9243.
- (45) Frisch, M. J.; Trucks, G. W.; Schlegel, H. B.; Scuseria, G. E.; Robb, M. A.; Cheeseman, J. R.; Scalmani, G.; Barone, V.; Mennucci, B.; Petersson, G. A.; Nakatsuji, H.; Caricato, M.; Li, X.; Hratchian, H. P.; Izmaylov, A. F.; Bloino, J.; Zheng, G.; Sonnenberg, J. L.; Hada, M.; Ehara, M.; Toyota, K.; Fukuda, R.; Hasegawa, J.; Ishida, M.; Nakajima, T.; Honda, Y.; Kitao, O.; Nakai, H.; Vreven, T.; Montgomery, J. A., Jr.; Peralta, J. E.; Ogliaro, F.; Bearpark, M.; Heyd, J. J.; Brothers, E.; Kudin, K. N.; Staroverov, V. N.; Kobayashi, R.; Normand, J.; Raghavachari, K.; Rendell, A.; Burant, J. C.; Iyengar, S. S.; Tomasi, J.; Cossi, M.; Rega, N.; Millam, J. M.; Klene, M.; Knox, J. E.; Cross, J. B.; Bakken, V.; Adamo, C.; Jaramillo, J.; Gomperts, R.; Stratmann, R. E.; Yazyev, O.; Austin, A. J.; Cammi, R.; Pomelli, C.; Ochterski, J. W.; Martin, R. L.; Morokuma, K.; Zakrzewski, V. G.; Voth, G. A.; Salvador, P.; Dannenberg, J. J.; Dapprich, S.; Daniels, A. D.; Farkas, O.; Foresman, J. B.; Ortiz, J. V.; Cioslowski, J.; Fox, D. J. *Gaussian 09, revision C.01*; Gaussian Inc., Wallingford, CT, 2010.
- (46) Zhao, Y.; Truhlar, D. G. *Theor. Chem. Acc.* **2008**, *120*, 215–241.
- (47) Zhao, Y.; Truhlar, D. G. *Acc. Chem. Res.* **2008**, *41*, 157–167.
- (48) Hehre, W. J.; Radom, L.; Schleyer, P. v. R.; Pople, J. A. *Ab Initio Molecular Orbital Theory*; Wiley: New York, 1986.
- (49) Chai, J.-D.; Head-Gordon, M. *Phys. Chem. Chem. Phys.* **2008**, *10*, 6615–6620.
- (50) Lan, Y.; Zou, L.-F.; Cao, Y.; Houk, K. N. *J. Phys. Chem. A* **2011**, *115*, 13906–13920.
- (51) Lazar, P.; Karlický, F.; Jurečka, P.; Kocman, M.; Otyepková, E.; Šafářová, K.; Otyepka, M. *J. Am. Chem. Soc.* **2013**, *135*, 6372–6377.
- (52) Bose, S.; Kuila, T.; Mishra, A. K.; Kim, N. H.; Lee, J. H. *Nanotechnology* **2011**, *22*, 405603.
- (53) Khanra, P.; Kuila, T.; Bae, S. H.; Kim, N. H.; Lee, J. H. *J. Mater. Chem.* **2012**, *22*, 24403–24410.
- (54) Mann, J. A.; Dichtel, W. R. *ACS Nano* **2013**, *7*, 7193–7199.
- (55) Kivala, M.; Diederich, F. *Acc. Chem. Res.* **2009**, *42*, 235–248.
- (56) Seo, J. M.; Jeon, I. Y.; Baek, J. B. *Chem. Sci.* **2013**, *4*, 4273–4277.
- (57) Jiang, D.; Sumpter, B. G.; Dai, S. *J. Chem. Phys.* **2007**, *126*, 134701.
- (58) Tang, Q.; Zhou, Z.; Chen, Z. F. *Nanoscale* **2013**, *5*, 4541–4583.
- (59) Wheland, G. W. *J. Am. Chem. Soc.* **1942**, *64*, 900–908.
- (60) Brown, R. D. *Q. Rev. Chem. Soc.* **1952**, *6*, 63–99.
- (61) <http://www.chem.ucalgary.ca/SHMO/>.